The C terminus of the mycobacterium ESX-1 secretion system substrate ESAT-6 is required for phagosomal membrane damage and virulence

Morwan M. Osman[1,2,5,#], Jonathan K. Shanahan[1,2,#], Frances Chu[3,6], Kevin K. Takaki[1,2], Malte L. Pinckert[1,2,7], Antonio J. Pagán[1,2], Roland Brosch[4], William H. Conrad[1,2,8], Lalita Ramakrishnan[1,2,3]*

[1] Molecular Immunity Unit, Cambridge Institute of Therapeutic Immunology and Infectious Diseases, Department of Medicine, University of Cambridge, CB2 OQH Cambridge, United Kingdom.

[2] Medical Research Council Laboratory of Molecular Biology, CB2 0QH Cambridge, United Kingdom.

[3] Department of Microbiology, University of Washington, Seattle, WA 98105, USA

[4] Institut Pasteur, Unit for Integrated Mycobacterial Pathogenomics, CNRS UMR3525, Paris, France

[5] Current address: York Structural Biology Laboratory, Department of Chemistry, University of York, York, YO10 5DD, UK

[6] Current address: TwinStrand Biosciences, Seattle, WA 98121, USA

[7] Current address: Department of Pathology, University of Cambridge, Cambridge, United Kingdom.

[8] Current address: Department of Chemistry, Lake Forest College, Lake Forest, Illinois, USA

[#]M.M.O and J.K.S contributed equally to this work

*Lalita Ramakrishnan

Email: lalitar@mrc-lmb.ac.uk

Author Contributions: W.H.C., M.M.O., J.K.S., M.L.P., A.J.P. and L.R. designed research; W.H.C., M.M.O., J.K.S., F.C., K.K.T., M.L.P. performed research; R.B. contributed new reagents/analytic tools; W.H.C., M.M.O., J.K.S., M.L.P., A.J.P., K.K.T., and L.R. analyzed data; M.M.O. and L.R. wrote the paper with input from W.H.C and J.K.S.; M.M.O. and K.K.T. prepared figures; All authors edited the paper.

Competing Interest Statement: We have no competing interests to declare.

Classification: Biological Sciences, Microbiology

Keywords: ESAT-6, ESX-1, tuberculosis, phagosomal damage, virulence

Abstract

Mycobacterium tuberculosis and its close relative *Mycobacterium marinum* infect macrophages and induce the formation of granulomas, organized macrophage-rich immune aggregates. These mycobacterial pathogens can accelerate and co-opt granuloma formation for their benefit, using the specialized secretion system ESX-1, a key virulence determinant. ESX-1-mediated virulence is attributed to the damage it causes to the membranes of macrophage phagosomal compartments, within which the bacteria reside. This phagosomal damage, in turn, has been attributed to the membranolytic activity of ESAT-6, the major secreted substrate of ESX-1. However, mutations that perturb ESAT-6's membranolytic activity often result in global impairment of ESX-1 secretion. This has precluded an understanding of the causal and mechanistic relationships between ESAT-6 membranolysis and ESX-1-mediated virulence. Here, we identify two conserved residues in the unstructured C-terminal tail of ESAT-6 required for phagosomal damage, granuloma formation and virulence. Importantly, these ESAT-6 mutants have near-normal levels of secretion, far higher than the minimal threshold we establish is needed for ESX-1-mediated virulence early in infection. Unexpectedly, these loss-of-function ESAT-6 mutants retain the ability to lyse acidified liposomes. Thus, ESAT-6's virulence functions *in vivo* can be uncoupled from this *in vitro* surrogate assay. These uncoupling mutants highlight an enigmatic functional domain of ESAT-6 and provide key tools to investigate the mechanism of phagosomal damage and virulence.

59 **Significance Statement**

60 Tuberculosis (TB), an ancient disease of humanity, continues to be a major cause of
61 worldwide death. The causative agent of TB, *Mycobacterium tuberculosis*, and its close
62 pathogenic relative *Mycobacterium marinum*, initially infect, evade, and exploit
63 macrophages, a major host defense against invading pathogens. Within macrophages,
64 mycobacteria reside within host membrane-bound compartments called phagosomes.
65 Mycobacterium-induced damage of the phagosomal membranes is integral to
66 pathogenesis, and this activity has been attributed the specialized mycobacterial secretion
67 system ESX-1, and particularly to ESAT-6, its major secreted protein. Here, we show
68 that the integrity of the unstructured ESAT-6 C-terminus is required for macrophage
69 phagosomal damage, granuloma formation, and virulence.

70

Main Text

Introduction

The type VII secretion system ESX-1 (ESAT-6 Secretion System 1) is a major virulence determinant in *Mycobacterium tuberculosis* (Mtb) and its close relative *Mycobacterium marinum* (Mm) (1-4). ESX-1 was identified as a virulence determinant when a 9.4 kb deletion in this region was discovered in the live attenuated tuberculosis vaccine Bacillus Calmette–Guérin (BCG) (2, 5). This "Region of Difference 1 (RD1)" was found to be required for both Mtb and Mm virulence (1, 2). The *esx-1* locus was then found to extend beyond RD1 in both organisms (6, 7) (Fig. S1A). Mtb and Mm ESX-1 systems are functionally equivalent: complementation of Mm−ΔRD1 with a cosmid containing the Mtb ESX-1 locus restores ESX-1 functions (8), and the use of Mm has facilitated fundamental discoveries about ESX-1 function (9). ESX-1 promotes virulence through an array of processes including activation of cytosolic signaling pathways, macrophage death, and pathogenic acceleration of tuberculous granulomas through induction of MMP9, which in turn promote mycobacterial growth (3, 9-12). ESX-1 also mediates damage of the macrophage phagosomal membranes in which the bacteria reside, and this is thought to be integral to ESX-1-mediated virulence (13-15).

ESX-1's membranolytic activity had been ascribed to its major secreted substrate ESAT-6 (6 kDa early secretory antigenic target) (16). ESAT-6 was discovered as a secreted, immunodominant Mtb antigen long before the *esx-1* locus was identified (17). Once the *esx-1* locus was identified, it was determined that the genes encoding ESAT-6 (*esxA*) and its secreted partner CFP-10 (*esxB*) reside in RD1 (Fig. S1A) (5, 6). ESAT-6 and CFP-10 (95 and 100 amino acids, respectively), were the first identified members of

94 the type VII secretion-associated WXG100 superfamily, so named for their conserved
95 WXG motif and their size of ~100 amino acids (18). Pinning down the role of ESAT-6
96 and other ESX-1 substrates in membranolysis and virulence has been complicated by
97 their co-dependency for secretion, as deletion of ESAT-6 causes loss of other ESX-1
98 substrates (19, 20). A separate line of evidence used purified recombinant ESAT-6 to
99 implicate it in membranolysis. Purified ESAT-6, but not its co-secreted partner CFP-10,
100 lysed artificial lipid bilayers, liposomes, and red blood cells (RBCs), leading to the
101 conclusion that ESAT-6 functions as a classical pore-forming toxin (15, 21, 22).
102 However, we and others found that many of the pore-forming activities ascribed
103 to ESAT-6, such as RBC lysis, was due to residual detergent contamination in ESAT-6
104 preparations made using standard, widely distributed protocols (8, 23, 24). Moreover, we
105 found that true ESX-1-mediated RBC lysis was contact-dependent and caused gross
106 membrane disruptions as opposed to distinct pores (8). These findings suggested that
107 ESAT-6 was either not directly involved in ESX-1 mediated membranolysis *in vivo* or
108 required additional mycobacterial factors. One such additional factor has been identified:
109 we and others have shown that the mycobacterial cell surface lipid phthiocerol
110 dimycocerosate (PDIM) is also required for macrophage phagosomal damage in both
111 Mtb and Mm (25-29). There is also increasing evidence that ESX-1 substrates other than
112 ESAT-6 are required for its pathogenic activity. Mm mutants in the ESX-1 genes *espE*
113 and *espF* secrete normal levels of ESAT-6 but are attenuated in ESX-1-mediated
114 virulence functions (30). These findings suggest that ESAT-6 is not sufficient for ESX-1
115 virulence function while leaving open the question of whether it is necessary. Continued
116 efforts to understand to what extent ESAT-6 is directly involved in ESX-1

117 membranolysis and virulence have not provided clear answers. Mm transposon mutants
118 have been identified that do not secrete ESAT-6 but are capable of damaging macrophage
119 phagosomes as evidenced by bacterial cytosolic translocation (31), and ESAT-6
120 secretion-deficient ESX-1 mutants have been identified that are unaffected in
121 intramacrophage growth and/or virulence in Mm and Mtb (32-36). These findings go
122 against a direct role for ESAT-6 in ESX-1's membranolytic activity. However, there is
123 also strong evidence supporting ESAT-6's direct involvement in ESX-1-mediated
124 membranolytic activity and virulence. Levels of surface-bound ESAT-6 correlate with
125 cytotoxicity and intramacrophage growth (35, 37). An N-terminal ESAT-6 point mutation
126 (Q5K) preserves ESAT-6 secretion but attenuates phagosomal permeabilization,
127 cytotoxicity and Mm growth in cultured macrophages, and zebrafish larvae (38).
128 Covalent modification of secreted ESAT-6 reduces hemolysis and intramacrophage
129 growth (39), suggesting that ESAT-6 functions as a secreted effector. ESAT-6 Q5K and
130 covalently modified ESAT-6 are both attenuated in ability to lyse acidified liposomes,
131 which is considered a proxy for its *in vivo* membranolytic activity. Lysis of acidified
132 liposomes is the single *in vitro* assay where both recombinant and natively purified Mtb
133 ESAT-6 exhibit membranolytic activity in the absence of contaminating detergent (21,
134 23, 40).

135 In this work, we probe the role of ESAT-6 in virulence. We find that mutation of
136 EccA1, a putative ESX-1 chaperone, or treatment with the drug ebselen results in a
137 drastic reduction in ESAT-6 and of its co-secreted partner, CFP-10. Both the *eccA1*
138 mutant and ebselen-treated Mm retain substantial phagosome-damaging activity, growth,
139 and granuloma formation *in vivo*. In contrast, we find that two C-terminal point mutations

140 in ESAT-6 allow substantial levels of ESAT-6 and CFP-10 secretion but cause complete
141 loss of phagosomal membrane damage and virulence. Moreover, mutation of the C-
142 terminus still allows for lysis of acidified liposomes, showing that there are additional
143 requirements for ESAT-6 mediated membrane damage *in vivo*.
144

145 **Results**

146 **Minimal ESAT-6 secretion suffices for ESX-1's pathogenic functions**

147 In prior work, we had found that a C-terminal M93T point mutation in ESAT-6
148 (Mm−ΔRD1::M93T_{mt}) resulted in greatly decreased secretion not only of ESAT-6, but
149 also of CFP-10 (8). As CFP-10 is dependent on ESAT-6 for secretion, this suggested that
150 the mutation might disrupt ESX-1 virulence simply by compromising ESAT-6-dependent
151 ESX-1 substrate secretion (8). However, Mm mutants in *eccA1*, which encodes the
152 AAA+ ATPase EccA1 – a putative chaperone for ESX-1 substrates – are also deficient
153 for ESAT-6 and CFP-10 secretion (7, 33) yet, they are reported to be only somewhat
154 compromised for virulence (33, 36). This suggested that minimal ESAT-6 secretion is
155 compatible with ESX-1 mediated virulence. To study the link between ESAT-6 secretion
156 and ESX-1-mediated virulence phenotypes, we examined a Mm transposon mutant in
157 *eccA1* (Mm-*eccA1*::Tn). We confirmed that Mm-*eccA1*::Tn had minimal ESAT-6 and
158 CFP-10 secretion, comparable to that of Mm−ΔRD1::M93T_{mt} (Fig. 1A and Fig. 3B) (8).
159 We also confirmed that Mm-*eccA1*::Tn was deficient for RBC lysis, as previously
160 reported (Fig. 1B) (7, 33). Next, we examined the extent to which Mm-*eccA1*::Tn could
161 damage phagosomal membranes by using the galectin-8 staining assay. This assay takes
162 advantage of the fact that cytosolic galectins bind to lumenal β-galactoside-containing

163 glycans that become exposed on damaged vesicles and can be visualized by
164 immunofluorescence microscopy (Fig. 1C) (28, 41, 42). Infection with Mm-*eccA1*::Tn
165 resulted in decreased galectin-8 puncta but substantially more than an Mm-ΔRD1 (26%
166 vs. 6.9% of wildtype puncta) (Fig. 1D). Also, as previously reported, Mm-*eccA1*::Tn had
167 only partially attenuated growth in cultured macrophages (Fig. 1E) (7, 33). It achieved
168 nearly wildtype bacterial burdens during zebrafish larval infection (0.82±0.16 fold of
169 wildtype vs 0.29±0.05 fold for Mm−ΔRD1) and this was associated with wildtype levels
170 of granuloma formation, an ESX-1-mediated phenotype (Fig. 1F-H) (3, 11, 12). Thus, the
171 reduction in ESAT-6 secretion resulting in *eccA1*::Tn abrogates RBC lysis but retains
172 significant phagosome-damaging activity and nearly wildtype levels of growth in human
173 and zebrafish macrophages, at least over the first few days of infection.
174 To further investigate the relationship between levels of ESAT-6 secretion,
175 membranolysis and virulence, we used the drug ebselen. Ebselen reduces ESAT-6
176 secretion in wildtype Mm to similar levels as Mm-*eccA1*::Tn albeit through an EccA1-
177 independent mechanism (43). Ebselen resulted in the same dissociation between ESAT-6
178 secretion and virulence phenotypes in wildtype Mm that we had observed for Mm-
179 *eccA1*::Tn., with inhibition of RBC lysis and phagosomal damage combined with a
180 minimal effect on intracellular bacterial growth (Fig. 1I-K). Zebrafish experiments with
181 ebselen were precluded by drug toxicity at concentrations exceeding 1 μM, a dose at
182 which ebselen shows no effect on ESX-1 function (43). In sum, minimal ESAT-6
183 secretion is sufficient to support some level of phagosomal damage, which, in turn, is
184 sufficient for substantial mycobacterial virulence at least early in infection. Given this
185 insight, the reduction in ESX-1 substrate secretion in Mm−ΔRD1::M93T_{mt} was not

186 sufficient to explain its complete loss of phagosomal damage and virulence, warranting
187 further investigation of the role of ESAT-6 and, particularly, its C-terminus.

188 **ESAT-6 C-terminal point mutants retain appreciable ESAT-6 secretion**

189 Residues 83-95 of ESAT-6 form a highly conserved C-terminal motif (Fig. 2A-C,
190 Fig. S3) (44). Our prior work on the effect of the ESAT-6 M93T mutation had used an
191 RD1 deletion mutant of Mm complemented with a cosmid containing the extended ESX-
192 1 region of Mtb expressing an ESAT-6 M93T mutant (Δ*esxA*::M93I_{Mtb}) (Fig. 2A-C, Fig.
193 S1). For a more refined analysis, we constructed an ESAT-6 deletion mutant
194 (Mm−Δ*esxA*) and complemented it using an integrating plasmid with wildtype ESAT-6
195 or ESAT-6 M93T mutation (Fig. S1). We also generated a second mutant of ESAT-6 in
196 this region, where another highly conserved methionine was changed to an isoleucine
197 (Δ*esxA*::M83I_{Mtb}) (Fig. 2A-C). Like the ESAT-6 M93T mutant, the ESAT-6 M83I
198 mutant also displayed reductions in secretion and intramacrophage growth in the context
199 of cosmid complementation of Mm-ΔRD1 (Fig. S2) (8, 45).

200 We found that Mm−Δ*esxA* had total loss of ESAT-6 and CFP-10 secretion,
201 similar to Mm−ΔRD1, and this was restored by *esxA* complementation (Fig. 3A).
202 Complementation of Mm−Δ*esxA* with ESAT6 M93T (Δ*esxA*::M93T_{Mtb}) restored
203 secretion to a substantial degree, more than the original cosmid complementation system
204 and much more than Mm-*eccA1*::Tn (Fig. 3A and B). Thus, the reduced secretion seen
205 with the cosmid complementation of Mm−ΔRD1 is likely an artifact of partial
206 complementation of the RD1 locus, gene dosage effects, subunit stoichiometry effects or
207 a combination of these that are mitigated by the current system. Importantly, the two C-
208 terminal mutations largely preserve ESAT-6 and CFP-10 secretion.

209 **ESAT-6 C-terminal point mutants lose membranolytic activity and virulence**

210 We could now use the two mutants to study the impact of ESAT-6 C-terminal
211 integrity on ESAT-6 membranolytic activity and virulence. We first ascertained that
212 Mm−Δ*esxA* was compromised for RBC lysis activity, phagosomal damaging activity,
213 macrophage growth, and growth and granuloma formation in zebrafish larvae, similar to
214 Mm−ΔRD1 (Fig. 4A-F) (8, 11, 28). All of these defects were rescued by
215 complementation with Mtb ESAT-6 (Mm−Δ*esxA*::WT_{Mtb}) (Fig. 4A-F). However, ESAT-
216 6 bearing either C-terminal mutation failed to complement any of the phenotypes. Thus,
217 the integrity of the ESAT-6 C terminus, while largely dispensable for secretion, is
218 absolutely required for phagosomal membrane damage, which, in turn, is linked to
219 granuloma formation and mycobacterial growth in vivo.

220 **The ESAT-6 M93T mutant retains wildtype levels of acidified liposome lysis activity**

221 Under acidic conditions (≤pH 5), ESAT-6 undergoes a conformational shift and
222 inserts into liposomal membranes, resulting in their lysis (16, 46). Based on these
223 observations, ESAT-6's lysis of acidified liposomes has been used as a proxy for its role
224 in phagosomal damage and permeabilization (16, 23). However, the relevance of the
225 liposome lysis assay for ESAT-6's role in phagosomal damage has been unclear. During
226 Mm and Mtb infection, inhibition of phagosomal acidification, using the vacuolar type
227 ATPase (v-ATPase) inhibitors bafilomycin A1 or concanamycin A, either has no effect
228 on or even enhances phagosomal permeabilization/damage (8, 26, 47, 48). However, it
229 has been argued that these findings may represent artifacts caused by alterations in
230 phagosomal membrane composition caused by chemical inhibition of v-ATPase (49). To
231 address the role of phagosomal acidification under natural conditions, we took advantage

232 of the observation that during macrophage infection, mycobacteria reside in both
233 acidified and nonacidified phagosomes (50). We found that 24 hours post-infection,
234 88.5% of Mm (415/469), were in acidified phagosomes as determined by staining with
235 LysoTracker, an acidophilic dye that labels lysosomal compartments (50). Co-staining
236 with galectin-8 showed that a significantly higher proportion of bacteria residing in
237 acidified phagosomes were positive (2-fold increase over nonacidified) (Fig. 5). To see if
238 phagosomal acidification also increases Mtb-mediated phagosomal damage, we used the
239 auxotrophic Mtb H37Rv strain, $mc^2$6206, a containment level 2 organism, which retains
240 ESX-1 function (43, 51, 52). After 24 hours, 67.4% (320/475) of the bacterial
241 phagosomes were acidified. As with Mm, there was significant increase in galectin-8
242 recruitment to bacteria residing in acidified compartments (1.7-fold increase over
243 nonacidified) (Fig. 5). These findings show that both Mm and Mtb ESAT-6-mediated
244 phagosomal damage is indeed enhanced by acidification.
245 Importantly, these findings re-enforced the argument that the lytic activity of
246 ESAT-6 on acidified liposomes is a proxy of ESAT-6-mediated phagosomal damage
247 (16). Our finding that the C-terminal mutants had almost no phagosomal damage (Fig.
248 4B), when most of the bacteria are in acidified phagosomes, indicated that they are
249 unable to damage phagosomes even under the sensitizing acidified condition. Therefore,
250 we expected that the C-terminal mutations would cause ESAT-6 to lose acidified
251 liposome lysis activity. We used recombinant ESAT-6-M93T, a less conservative
252 mutation than M83I, which we hypothesized to be more likely to disrupt ESAT-6
253 function. To measure lysis, we generated 1,2-Dioleoyl-sn-glycero-3-phosphocholine
254 (DOPC) liposomes containing the fluorescent dye 8-Aminonaphthalene-1,3,6-Trisulfonic

255 acid (ANTS), a formulation which has been used for previous systematic analyses of
256 ESAT-6's lytic activity (46, 53). We were surprised to find that ESAT-6-M93T retained
257 wildtype levels of acidified lysis (Fig. 6). This stood in contrast to the prior findings that
258 recombinant ESAT-6 containing the N-terminal Q5K mutation, which caused loss in
259 phagosomal damage in Mm, was found to be deficient in lysis of acidified DOPC
260 liposomes (38). Thus, our finding uncouples ESAT-6's *in vitro* and *in vivo* membrane-
261 damaging activities even under acidified conditions, suggesting an *in vivo* role for
262 specific residues in the C terminus.

263 **Discussion**

264 This work was instigated by our finding that barely detectable levels of ESAT-6
265 secretion in both an Mm *eccA1* mutant and ebselen treated Mm only halved ESX-1-
266 mediated phagosomal membrane. In turn, this level of phagosomal damage was sufficient
267 for relatively high levels of *in vivo* growth compared to ESX-1 deficient Mm. Our
268 findings led us to revisit our previous conclusions that an ESAT-6 C-terminal point
269 mutation (ESAT-6 M93T) lost phagosomal membrane damage and early virulence solely
270 due to reduced secretion (8). The Mm-ESAT-6 M93T mutant allowed for much greater
271 levels of ESAT-6 secretion than the Mm-*eccA1*::Tn mutant, showing that ESAT-6 C-
272 terminal integrity was needed for ESAT-6's direct membrane damaging and virulence
273 effects. We solidified this conclusion through experiments demonstrating that the Mm-
274 ESAT-6 M83I mutant had a similar dissociation between secretion and virulence
275 phenotypes. In the course of this analysis, we found that *in vivo* ESAT-6-mediated
276 phagosomal lysis by Mtb and Mm was enhanced in acidic compartments. This suggested
277 that the pH-dependent lytic activity of purified ESAT-6 was a direct correlate of

278 phagosomal damage. However, we found that purified ESAT-6-M93T retained full
279 activity in lysing acidified liposomes.

280 Previous studies examining both transposon mutants and total knockouts of *eccA1*
281 have found defects in hemolysis and *in vivo* growth similar to those we observed in Mm-
282 *eccA1*::Tn (7, 36). A genome-wide Mtb transposon mutant screen in both cultured
283 macrophages and the mouse TB model identified *eccA1*::Tn mutants as being attenuated
284 (54-56). These findings are broadly consistent with ours, although in the absence of direct
285 comparisons, it is not clear whether EccA1 is less important than the full ESX-1 locus in
286 Mtb infection as well. Our findings that minimal ESAT-6 secretion is compatible with
287 substantial preservation of early Mm infection phenotypes are also in line with prior
288 observations of phagosomal damage (as reflected by cytosolic translocation of
289 mycobacteria) in ESAT-6 secretion-deficient Mm mutants (31). We see two possible
290 explanations for this. First, minute amounts of secretion that are not detected by
291 immunoblotting could be sufficient for ESX-1 function (32, 57). Second, surface-bound
292 ESAT-6 can partially compensate for the lack of secretion during early infection. Two
293 studies have found that the retention of surface-bound ESAT-6 correlates with pathogenic
294 phenotypes (35, 37). Furthermore, an earlier report on Δ*eccA1* found wildtype levels of
295 ESAT-6 in bacterial cell surface extracts despite an overall reduction in ESX-1 secretion
296 (36).

297 ESAT-6 binds to CFP-10 to form a heterodimeric complex and the two proteins
298 are likely co-secreted (58). ESAT-6's C-terminus does not participate in binding to CFP-
299 10 (Fig. 2A) and truncation of this region (Δ84-95) does not affect secretion, likely as
300 CFP-10's C-terminal tail is responsible for recognition and secretion of the heterodimer

301 (58-61). However, conservation of ESAT-6's C-terminus among mycobacterial homologs
302 (Fig. S3), suggests it mediates an essential function beyond secretion. Consistent with
303 this, an Mtb mutant expressing the C-terminal ESAT-6 truncation has reduced
304 phagosomal permeabilization as reflected by translocation into the cytosol (59).
305 Furthermore, it was reported that complementation of *M. bovis* BCG with an ESX-1
306 cosmid expressing truncated ESAT-6 did not rescue attenuation (45). This region appears
307 to be highly conserved in clinical strains: we examined the GMTV database of 2,819 Mtb
308 isolates for occurrences of nonsynonymous (coding) mutations in *esxA*, and of the 8
309 occurrences of nonsynonymous mutations in *esxA*, none were in located in the conserved
310 C-terminal motif (residues 83-95) (62).
311 Our finding that phagosomal acidification greatly enhances ESAT-6-mediated
312 damage supports the model that ESAT-6's pH-dependent functions *in vitro* are
313 physiologically relevant (16, 21, 40). This assay does not fully capture ESAT-6's *in vivo*
314 role, as mycobacteria in non-acidified compartments still induced phagosomal damage to
315 a greater extent than either of the C-terminal ESAT-6 mutants. However, it is likely that
316 ESAT-6's activity under acidic pH mimics an aspect of its *in vivo* function. This is
317 further supported by the recent finding that membrane vesicles prepared using lipids from
318 the THP-1 human monocytic cell line are also damaged by ESAT-6 (recombinant and
319 native) only at acidic pH (23, 26). On this backdrop, it is interesting to consider the role
320 of the ESAT-6 C terminus in phagosomal damage, particularly of the two point mutants
321 examined here. It has been shown that in the context of acidified liposome lysis, the
322 ESAT-6 C-terminus does not insert into the membrane and remains solvent exposed (46).
323 NMR and crystal structures of the heterodimer predict that the tail is floppy and

324 unstructured (44, 58). However, the authors who solved the crystal structure suggested
325 that this region could also adopt an alpha helical structure *in vivo* (44). This was based on
326 identification of a C-terminal motif conserved across actinobacterial ESAT-6 homologs
327 that is consistent with an alpha helical structure (44). This hypothesis is supported by the
328 recent AlphaFold2 structural prediction of ESAT-6 with a structured C terminus (63)
329 (Fig. 2C). This disparity between experimental and predicted structure could reflect a
330 conformational versatility of the C-terminus that is required for different aspects of
331 ESAT-6's *in vivo* functions.

332 The ESAT-6 C-terminal tail resides on the exterior of lipid membranes following
333 insertion (46). While an ESAT-6 C-terminal truncation mutant can insert into liposome
334 membranes, it has reduced lytic activity (46). This suggests a direct role for the C
335 terminus in enabling "basal" ESAT-6 membranolytic function. The ESAT-6 M93T and
336 M83I point mutants are relatively conservative. As methionine and isoleucine are both
337 small hydrophobic residues, an isoleucine mutation is highly conservative, while
338 threonine, as a small polar residue would be less so. Neither of these mutations would be
339 predicted to be particularly disruptive to C-terminal structure, and in this light, perhaps it
340 is not surprising after all that the M93T mutation does not affect its *in vitro* basal
341 membranolytic activity. Rather, this finding suggests that the M93T mutant is defective
342 in a C-terminally mediated function that is required for robust *in vivo* lysis. Following
343 membrane insertion, the C-terminus could enhance oligomerization of ESAT-6,
344 interactions with mycobacterial or host factors, or act as a bacterial sensor for contact-
345 dependent lysis by ESX-1, or any combination of these. Putative mycobacterial factors
346 include other ESX-1 substrates that contribute to virulence in addition to ESAT-6, such

347 as EspA, EspE, or EspF (9, 32, 64), or oligomers of EspB and EspC which are proposed
348 to be part of a putative extracellular secretory complex mediating contact-dependent lysis
349 (65, 66). A systematic mutational analysis of the C terminus coupled with biochemical
350 studies to identify mycobacterial, or possibly even host, determinants that bind to
351 wildtype but not M93T and other *in vivo* deficient ESAT-6 mutants may pave the way to
352 a fuller understanding of ESAT-6's *in vivo* function.

353 **Materials and Methods**

354 **Bacterial strains and culture methods**

355 All Mm and Mtb strains used are listed in Table S3. Mm strains were all derived from
356 wildtype Mm purchased from American Type Culture Collection (strain M, ATCC
357 #BAA-535). Mm strains were grown without agitation at 33°C in 7H9 Middlebrook's
358 medium (Difco) supplemented with 10% OADS and 0.05% Tween®80 (Sigma) with
359 appropriate selection [50 µg /mL hygromycin (Mediatech) and 20 µg /mL kanamycin
360 (Sigma)] or on supplemented Middlebrook 7H10 agar (Millipore) [no Tween®80] (67).
361 Mtb $mc^2$6206 strains (51) were grown without agitation at 37ºC in 7H9 Middlebrook's
362 medium (Difco) supplemented with 10% OADC (Becton Dickinson), 0.05% Tween®80
363 (Sigma), 12 µg/mL pantothenic acid (Sigma) and 25 µg /mL L-leucine (Sigma) with
364 appropriate selection [20 µg /mL kanamycin (Sigma)] or on supplemented Middlebrook
365 7H10 agar (Millipore) [no Tween®80].

366 **Generation of mutant strains**

367 The *eccA1*::Tn mutant was isolated from a Mm transposon mutant library. Briefly, a
368 novel *mariner*-based mini transposon containing an excisable hygromycin-resistance

369 cassette was used to mutagenize wildtype Mm in small batches and individual colonies
370 were isolated and sequenced. The transposon insertion in *eccA1*::Tn was confirmed by
371 semi random, nested PCR and was located 16.26% into the *eccA1* open reading frame, as
372 measured by distance from the ATG start site.
373 The Mm-Δ*esxA* mutant was generated using phage transduction (68). Briefly, a fragment
374 containing sequences flanking *esxA* (23-955 bp upstream of the ATG, 13-1101 bp and
375 downstream of its stop codon) were cloned into pYUB854 to generate pYUB854-*esxA*.
376 The resulting cosmid was digested with PacI (NEB) and the insert was ligated into
377 phAE159 (a gift from William Jacobs) to generate the phSP105 phasmid. Following
378 ligation, packaging, and transduction, phSP105 was transformed into *M. smegmatis*
379 mc^2155. Harvested phages were transduced into wildtype Mm and plated on 7H10-Hyg.
380 Positive colonies were confirmed by southern blotting, and the hygromycin cassette was
381 excised via transformation with pYUB870. Loss of pYUB870 was confirmed by plating
382 on 7H10+sucrose plates, and excision of cassette confirmed via PCR.

383 **Complementation Constructs**

384 Mm-Δ*esxA* was complemented with pMH406 (69). ESAT-6-M83I and ESAT-6-M93T
385 complementation constructs (Table S1) were generated via site directed mutagenesis
386 using primers listed in Table S2.

387 **Single-cell suspensions of mycobacteria**

388 Single-cell suspensions of mycobacteria were prepared as previously described (67), with
389 minor modifications. Briefly, mycobacteria were cultured with antibiotic selection to
390 mid-log (OD_{600} = 0.3 – 0.6) and then pelleted at 3,220 x g for 20 minutes at 20°C. The
391 top layer of the pellet containing precipitated kanamycin was discarded following gentle

392 scraping with a disposable inoculating loop. The underlying pellet was resuspended in 5
393 mL 7H9 media supplemented with 10% OADS (no Tween®80) and then passed 10 times
394 through a 27-gauge blunt needle. Mycobacteria were then pelleted at 100 x g for 1
395 minute. A total of 4 mL supernatant was collected. The bacterial pellet was resuspended
396 in 5 mL of 7H9 OADS. Mycobacteria were again passed 10 times through a blunt needle,
397 pelleted at 100 x g, and supernatant collected. This was repeated until 15 mL supernatant
398 was collected. The supernatant was then passed through a 5 µm syringe filter (Pall, 4650)
399 to isolate single-cell bacteria. Single-cell bacteria were concentrated by centrifugation at
400 3,220 x g for 30 minutes at room temperature. The pellet was then resuspended in 200 µL
401 7H9 OADS, divided into 5 µL aliquots, and stored at −80°C. Mycobacterial
402 concentration was determined by plating for CFU.

403 **Intramacrophage growth assays**

404 Growth assays were performed as described previously with minor modifications (8).
405 J774A.1 cells were maintained in Gibco Dulbecco's Modified Eagle Medium (DMEM).
406 24 hours before infection, cells were scraped and resuspended in DMEM to a
407 concentration of 2.5 x 10^5 cells/mL. J774A.1s were plated in a 24-well optical bottom
408 tissue culture plate (Perkin Elmer, 1450-606) by aliquoting 500 µL of this cell suspension
409 to each well and then incubating at 37°C overnight. The following day, cells were
410 washed twice with PBS and infected with antibiotic-free media containing single-cell
411 suspensions of tdTomato-expressing Mm at a multiplicity of infection of ~0.25 (wildtype,
412 *eccA1*::Tn, ::*esxA*) or ~0.5 (attenuated strains) for 4 hours at 33ºC, 5% CO_2. After
413 infection, cells were washed twice with PBS, 500 µL fresh media added to each well and
414 then incubated at 33°C, 5% CO_2. Cells were imaged by fluorescence microscopy at

415 indicated timepoints using a Nikon Eclipse Ti-E equipped with a Ti-S-E Motor XY
416 Stage, a C-HGFIE 130-W mercury light source, a 23/0.10 Plan Apochromat objective,
417 and a Chroma ET-CY3 (49004) filter cube. Fluorescence images were captured with a
418 Photometrics CoolSNAP HQ2 Monochrome Camera, using NIS-Elements (version 3.22).
419 Resulting images were analyzed in ImageJ using a custom script for fluorescence pixel
420 count (FPC), to determine bacterial burden (67).

421 **Galectin-8 immunofluorescence**

422 THP-1 cells were diluted to 5 x 10^5 cells/mL in RPMI + 10% FCS (Gibco) and treated
423 with 100 nM phorbol 12-myrystate-13-acetate (PMA) (Sigma, P1585). THP-1 cells were
424 plated in a 24-well optical bottom tissue culture plate (Perkin Elmer, 1450-606) by
425 aliquoting 500 µL of this cell suspension to each well and then incubating at 37°C for two
426 days. PMA-containing media was then removed and replaced with fresh media, and the
427 cells were allowed to rest for a day. The following day, cells were washed twice with
428 PBS and infected with antibiotic-free media containing single-cell suspensions of
429 tdTomato-expressing Mm at a multiplicity of infection of ~1 for 4 hours at 33ºC, 5%
430 CO_2. After infection, cells were washed twice with PBS, 500 µL fresh media added to
431 each well and then incubated overnight at 33°C, 5% CO_2.
432 Galectin-8 staining was done as previously described (28). Briefly, 24 hours after
433 infection, cells were fixed in 4% (wt/vol) paraformaldehyde in PBS at room temperature
434 for at least 30 minutes. Fixed cells were washed twice with PBS and then incubated in
435 permeabilization/block (PB) buffer for 30 minutes at room temperature, and then stained
436 with goat anti-human galectin-8 antibody (R&D Systems, AF1305) diluted in PB solution
437 overnight at 4°C. Cells were then washed three times with PBS and stained with

438 AlexaFluor488-conjugated donkey anti-goat IgG (ThermoFisher, A-11055) diluted in PB
439 solution for one hour at room temperature. Cells were then washed three times in PBS
440 and imaged.
441 LysoTracker experiments were conducted as above with the following modifications:
442 cells were infected with EBFP2-expressing Mm or Mtb at an MOI of ~0.5. The next day,
443 cells were stained with 100 nM of LysoTracker Red DND-99 (Invitrogen) in RPMI for
444 45 minutes at 33ºC, and then immediately fixed and stained as above. Acidic organelles,
445 fluorescent bacteria, and galectin-8 puncta were identified using the 3D surface rendering
446 feature of Imaris (Bitplane Scientific Software). Bacteria were scored as galectin-8
447 positive if they were located within 2 µm of a galectin-8 surface and as acidified if they
448 were located within a LysoTracker surface.

449 **Zebrafish Husbandry**

450 All zebrafish husbandry and experiments were performed in compliance with the UK
451 Home Office and the Animal Ethics Committee of the University of Cambridge.
452 Zebrafish maintenance and spawning was performed as previously described (67).
453 Briefly, zebrafish were maintained on a recirculating aquaculture system with a 14 hour
454 light – 10 hour dark cycle. Fish were fed dry food and brine shrimp twice a day. Adult
455 wildtype AB zebrafish were spawned, embryos collected and then housed in fish water
456 (reverse osmosis water containing 0.18 g/L Instant Ocean) at 28.5°C. The fish water was
457 supplemented with 0.25 µg/ml methylene blue from collection to 1 day post-fertilization
458 (dpf), and at 1 dpf 0.003% PTU (1-phenyl-2-thiourea, Sigma) was added to prevent
459 pigmentation.

460 **Zebrafish Infections**

461 Zebrafish larvae were infected with the indicated strains of tdTomato-expressing Mm by
462 injection into the caudal vein at 2 dpf using freshly thawed single-cell suspensions diluted
463 to the same CFU / µL. Injection dose was plated on 7H10 + 10% OADS with appropriate
464 antibiotic to ensure similar infection dose.

465 **Measuring Bacterial Burden in Larvae**

466 Fluorescence microscopy was performed as previously described (67). Briefly, infected
467 larvae were imaged by fluorescence microscopy at 5 days post-infection using a Nikon
468 Eclipse Ti-E equipped with a Ti-S-E Motor XY Stage, a C-HGFIE 130-W mercury light
469 source, a 23/0.10 Plan Apochromat objective, and a Chroma ET-CY3 (49004) filter cube.
470 Fluorescence images were captured with a Photometrics CoolSNAP HQ2 Monochrome
471 Camera, using NIS-Elements (version 3.22). The resulting images were analyzed in
472 ImageJ using a custom script for fluorescence pixel count (FPC), to determine bacterial
473 burden and infection foci size.

474 **Secretion Assay**

475 Culture filtrate (CF) fractions and cell pellet (CP) fractions were prepared as described
476 previously (8). Mm was grown to mid to late log stage, washed with PBS, resuspended to
477 a final OD600 of 0.8-1.0 in 50 mL of modified Sauton's Media, and incubated for 48
478 hours at 33°C. 10 µg of CP and 20 µg of CF were loaded per well for SDS-PAGE, and
479 presence of ESAT-6, CFP-10 and GroEL2 were determined by western blotting with
480 mouse anti-ESAT-6 clone 11G4 (1:3000; Thermo Fisher, HYB-076-08-02), rabbit anti-
481 CFP-10 (1:5000; BEI, product NR13801), or mouse anti-GroEL2 clone IT-56 (1:1000;
482 BEI, product NR-13655) primary antibody followed by HRP-conjugated goat anti-mouse

483 (1:10,000; Stratech 115- 035-003-JIR) (Fig. 3B and S2), goat anti-mouse IgG DyLight™
484 800 (1:15,000 Cell Signaling Technology #5257S), or goat anti-rabbit IgG DyLight™
485 800 (1:15,000 Cell Signaling Technology #5151S) secondary antibody.
486 Chemiluminescence detection was then performed using Amersham ECL Western
487 Blotting Detection Reagents (GE Lifesciences) and fluorescence imaging performed on a
488 LI-COR Odyssey.

489 **Hemolysis Assay**

490 Hemolytic activity was assessed as described previously (8). Briefly, 100 µL of 1% (v/v)
491 sheep red blood cells (RBC) (Fisher Scientific) in PBS was combined with 100 µL of
492 PBS, bacterial suspension or 0.1% Triton X-100 (Sigma), pelleted, and then incubated for
493 two hours at 33°C. Pellets were resuspended, re-pelleted and the absorbance of the
494 supernatant measured at 405 nm. Raw absorbance data were converted to percentage
495 lysis, by subtracting PBS lysis (background lysis) and dividing by 0.1% Triton X-100
496 lysis (complete lysis).

497 **Protein Expression & Purification**

498 Expression of recombinant ESAT-6 was conducted as previously (8) with the following
499 modifications: Bacterial pellets were resuspended in 5 mL of Lysis Buffer (150 mM
500 NaCl, 20 mM Tris pH 8, 5 mM Imidazole) per gram of pellet, and then sonicated on ice.
501 Lysates were clarified by centrifugation at 15,000 x g for 30 minutes at 4°C. Clarified
502 lysate was added to 1 mL of washed Ni-NTA bead slurry (Qiagen) and incubated for 1
503 hour at 4ºC. Beads were then pelleted and washed with 10 column volumes (CVs) of
504 lysis buffer. Next, beads were washed with 10 CV of binding buffer (150 mM NaCl, 20
505 mM Tris pH 8, 20 mM Imidazole), followed by 15 CV of wash buffer (150 mM NaCl, 20

506 mM Tris pH 8, 75 mM Imidazole). 3 CV of elution buffer (150 mM NaCl, 20 mM Tris
507 pH 8, 1 M Imidazole) was added to elute protein. Eluate was concentrated and then
508 loaded on a S75 size exclusion column (GE Healthcare) equilibrated with 150 mM NaCl,
509 20 mM Tris pH 8. Fractions were collected and monitored for recombinant protein
510 elution and purity by SDS-PAGE followed by Coomassie staining. Protein concentration
511 from highly purified eluted fractions were quantified by absorbance at 280 nm.
512 Constructs for mutant protein purification (Table S1) were generated via site directed
513 mutagenesis using listed primers (Table S2).

514 **Liposome Lysis Assay**

515 Liposomes containing 8-Aminonaphthalene-1,3,6-Trisulfonic Acid (ANTS) were
516 generated as previously described with modifications (8). Briefly, 1,2-dioleoyl-sn-
517 glycero-3-phosphocholine (Sigma) was dissolved in 86 µL of chloroform (Sigma) to 100
518 mg/mL. The resulting solution was transferred to a glass vial and chloroform evaporated
519 under N_2 gas and subsequently under vacuum overnight. Lipid films were resuspended in
520 400 µL of 125 mM ANTS (Invitrogen) in PBS by vortexing. Liposomes were generated
521 by five freeze-thaw cycles by freezing in liquid nitrogen for three minutes and then
522 thawing in a 40-50ºC water bath for three minutes. Liposomes were then extruded
523 twenty-five times through two 200 nm polycarbonate Nuclepore™ filters (Whatman) and
524 then washed in PBS by centrifugation at 60,000 × g for 30 minutes at 4°C. Liposomes
525 were resuspended in 400 µL PBS for use in assays.
526 Stock solutions of 200 mM sodium phosphate and 100 mM citric acid with 150 mM
527 NaCl were used to generate pH 4.5 and 7.4 phosphate-citrate pH buffers (pH buffer). The
528 pH value of each buffer was confirmed after preparation. To measure liposome lytic

529 activity of recombinant proteins, 5 μL of liposomes were resuspended in 200 μL pH
530 buffer and 3 μM rESAT-6 or an equivalent volume of vehicle was added. Protein and
531 liposome samples incubated with rotation at 20°C for 30 minutes in ultracentrifuge tubes.
532 Intact liposomes were pelleted by centrifugation at 180,0000 × g for 30 minutes at 4°C
533 and then ANTS fluorescence in the supernatants was measured [excitation/emission
534 (nm): 350 ± 15/520 ± 15]. Raw fluorescence data were converted to percentage of lysis,
535 by subtracting buffer only lysis (background lysis) and dividing by 0.05% Triton X-100
536 lysis (complete lysis) at each pH.

537 **Acknowledgments**

538 We thank R. Hegde for insights and discussion and J. Blaza for support and
539 encouragement. The following reagents were obtained through the NIH Biodefense and
540 Emerging Infections Research Resources Repository, NIAID, NIH: monoclonal anti-
541 Mycobacterium tuberculosis GroEL2 (gene Rv0440), clone CS-44 (produced in vitro),
542 NR-13813. *M. tuberculosis* mc^{2}6206 was a gift from William Jacob, pMH406 was a gift
543 from David Sherman.
544 This work was funded by Wellcome Trust Principal Research Fellowship (223103/
545 Z/21/Z) and the NIH MERIT award (R37 AI054503). For the purpose of open access,
546 the author has applied a CC BY public copyright licence to any Author Accepted
547 Manuscript version arising from this submission. This work is licensed under a
548 Creative Commons Attribution 4.0 International License.

549 **References**

550 1. K. N. Lewis *et al.*, Deletion of RD1 from Mycobacterium tuberculosis mimics
551 bacille Calmette-Guerin attenuation. *Journal of Infectious Diseases* **187**, 117-123
552 (2003).
553 2. A. S. Pym, P. Brodin, R. Brosch, M. Huerre, S. T. Cole, Loss of RD1 contributed
554 to the attenuation of the live tuberculosis vaccines Mycobacterium bovis BCG
555 and Mycobacterium microti. *Mol Microbiol* **46**, 709-717 (2002).
556 3. H. E. Volkman *et al.*, Tuberculous granuloma formation is enhanced by a
557 mycobacterium virulence determinant. *PLoS Biol* **2**, e367 (2004).
558 4. P. Brodin, I. Rosenkrands, P. Andersen, S. T. Cole, R. Brosch, ESAT-6 proteins:
559 protective antigens and virulence factors? *Trends Microbiol* **12**, 500-508 (2004).
560 5. G. G. Mahairas, P. J. Sabo, M. J. Hickey, D. C. Singh, C. K. Stover, Molecular
561 analysis of genetic differences between Mycobacterium bovis BCG and virulent
562 M. bovis. *J Bacteriol* **178**, 1274-1282 (1996).
563 6. W. Bitter *et al.*, Systematic genetic nomenclature for type VII secretion systems.
564 *PLoS Pathog* **5**, e1000507 (2009).
565 7. L. Y. Gao *et al.*, A mycobacterial virulence gene cluster extending RD1 is
566 required for cytolysis, bacterial spreading and ESAT-6 secretion. *Mol Microbiol*
567 **53**, 1677-1693 (2004).
568 8. W. H. Conrad *et al.*, Mycobacterial ESX-1 secretion system mediates host cell
569 lysis through bacterium contact-dependent gross membrane disruptions. *Proc Natl*
570 *Acad Sci U S A* **114**, 1371-1376 (2017).

571 9. A. E. Chirakos, A. Balaram, W. Conrad, P. A. Champion, Modeling Tubercular
572 ESX-1 Secretion Using Mycobacterium marinum. *Microbiol Mol Biol Rev* **84**
573 (2020).
574 10. C. J. Cambier, S. Falkow, L. Ramakrishnan, Host evasion and exploitation
575 schemes of Mycobacterium tuberculosis. *Cell* **159**, 1497-1509 (2014).
576 11. H. E. Volkman *et al.*, Tuberculous granuloma induction via interaction of a
577 bacterial secreted protein with host epithelium. *Science* **327**, 466-469 (2010).
578 12. J. M. Davis, L. Ramakrishnan, The role of the granuloma in expansion and
579 dissemination of early tuberculous infection. *Cell* **136**, 37-49 (2009).
580 13. R. Simeone, L. Majlessi, J. Enninga, R. Brosch, Perspectives on mycobacterial
581 vacuole-to-cytosol translocation: the importance of cytosolic access. *Cell*
582 *Microbiol* **18**, 1070-1077 (2016).
583 14. N. van der Wel *et al.*, M. tuberculosis and M. leprae translocate from the
584 phagolysosome to the cytosol in myeloid cells. *Cell* **129**, 1287-1298 (2007).
585 15. J. Smith *et al.*, Evidence for pore formation in host cell membranes by ESX-1-
586 secreted ESAT-6 and its role in Mycobacterium marinum escape from the
587 vacuole. *Infect Immun* **76**, 5478-5487 (2008).
588 16. Y. Bao, L. Wang, J. Sun, A Small Protein but with Diverse Roles: A Review of
589 EsxA in Mycobacterium-Host Interaction. *Cells* **10** (2021).
590 17. A. L. Sorensen, S. Nagai, G. Houen, P. Andersen, A. B. Andersen, Purification
591 and characterization of a low-molecular-mass T-cell antigen secreted by
592 Mycobacterium tuberculosis. *Infect Immun* **63**, 1710-1717 (1995).

588 18. M. J. Pallen, The ESAT-6/WXG100 superfamily -- and a new Gram-positive
589 secretion system? *Trends Microbiol* **10**, 209-212 (2002).
590 19. M. M. Champion, E. A. Williams, R. S. Pinapati, P. A. Champion, Correlation of
591 phenotypic profiles using targeted proteomics identifies mycobacterial esx-1
592 substrates. *J Proteome Res* **13**, 5151-5164 (2014).
593 20. S. M. Fortune *et al.*, Mutually dependent secretion of proteins required for
594 mycobacterial virulence. *Proc Natl Acad Sci U S A* **102**, 10676-10681 (2005).
595 21. M. I. de Jonge *et al.*, ESAT-6 from Mycobacterium tuberculosis dissociates from
596 its putative chaperone CFP-10 under acidic conditions and exhibits membrane-
597 lysing activity. *J Bacteriol* **189**, 6028-6034 (2007).
598 22. T. Hsu *et al.*, The primary mechanism of attenuation of bacillus Calmette-Guerin
599 is a loss of secreted lytic function required for invasion of lung interstitial tissue.
600 *Proc Natl Acad Sci U S A* **100**, 12420-12425 (2003).
601 23. J. Augenstreich *et al.*, Phthiocerol Dimycocerosates From Mycobacterium
602 tuberculosis Increase the Membrane Activity of Bacterial Effectors and Host
603 Receptors. *Front Cell Infect Microbiol* **10**, 420 (2020).
604 24. Y. Bao *et al.*, Mycobacterial surface-associated ESX-1 virulence factors play a
605 role in mycobacterial adherence and invasion into lung epithelial cells. *bioRxiv*
606 (2020).
607 25. A. K. Barczak *et al.*, Systematic, multiparametric analysis of Mycobacterium
608 tuberculosis intracellular infection offers insight into coordinated virulence. *PLoS*
609 *Pathog* **13**, e1006363 (2017).

610 26. J. Augenstreich *et al.*, ESX-1 and phthiocerol dimycocerosates of Mycobacterium
611 tuberculosis act in concert to cause phagosomal rupture and host cell apoptosis.
612 *Cell Microbiol* **19** (2017).
613 27. J. Quigley *et al.*, The Cell Wall Lipid PDIM Contributes to Phagosomal Escape
614 and Host Cell Exit of Mycobacterium tuberculosis. *mBio* **8** (2017).
615 28. M. M. Osman, A. J. Pagan, J. K. Shanahan, L. Ramakrishnan, Mycobacterium
616 marinum phthiocerol dimycocerosates enhance macrophage phagosomal
617 permeabilization and membrane damage. *PLoS One* **15**, e0233252 (2020).
618 29. T. R. Lerner *et al.*, Phthiocerol dimycocerosates promote access to the cytosol and
619 intracellular burden of Mycobacterium tuberculosis in lymphatic endothelial cells.
620 *BMC Biol* **16**, 1 (2018).
621 30. A. E. Chirakos, K. R. Nicholson, A. Huffman, P. A. Champion, Conserved ESX-1
622 Substrates EspE and EspF Are Virulence Factors That Regulate Gene Expression.
623 *Infect Immun* **88** (2020).
624 31. J. Lienard *et al.*, The Mycobacterium marinum ESX-1 system mediates
625 phagosomal permeabilization and type I interferon production via separable
626 mechanisms. *Proc Natl Acad Sci U S A* **117**, 1160-1166 (2020).
627 32. J. M. Chen *et al.*, Phenotypic profiling of Mycobacterium tuberculosis EspA point
628 mutants reveals that blockage of ESAT-6 and CFP-10 secretion in vitro does not
629 always correlate with attenuation of virulence. *J Bacteriol* **195**, 5421-5430 (2013).
630 33. S. A. Joshi *et al.*, EccA1, a component of the Mycobacterium marinum ESX-1
631 protein virulence factor secretion pathway, regulates mycolic acid lipid synthesis.
632 *Chem Biol* **19**, 372-380 (2012).

633 34. R. E. Bosserman, K. R. Nicholson, M. M. Champion, P. A. Champion, A New
634 ESX-1 Substrate in Mycobacterium marinum That Is Required for Hemolysis but
635 Not Host Cell Lysis. *J Bacteriol* **201** (2019).
636 35. G. M. Kennedy, G. C. Hooley, M. M. Champion, F. Mba Medie, P. A. Champion,
637 A novel ESX-1 locus reveals that surface-associated ESX-1 substrates mediate
638 virulence in Mycobacterium marinum. *J Bacteriol* **196**, 1877-1888 (2014).
639 36. T. H. Phan *et al.*, EspH is a hypervirulence factor for Mycobacterium marinum
640 and essential for the secretion of the ESX-1 substrates EspE and EspF. *PLoS*
641 *Pathog* **14**, e1007247 (2018).
642 37. J. Raffetseder, N. Iakobachvili, V. Loitto, P. J. Peters, M. Lerm, Retention of
643 EsxA in the Capsule-Like Layer of Mycobacterium tuberculosis Is Associated
644 with Cytotoxicity and Is Counteracted by Lung Surfactant. *Infect Immun* **87**
645 (2019).
646 38. Q. Zhang *et al.*, EsxA membrane-permeabilizing activity plays a key role in
647 mycobacterial cytosolic translocation and virulence: effects of single-residue
648 mutations at glutamine 5. *Sci Rep* **6**, 32618 (2016).
649 39. Y. Bao, L. Wang, J. Sun, Post-translational knockdown and post-secretional
650 modification of EsxA determine contribution of EsxA membrane permeabilizing
651 activity for mycobacterial intracellular survival. *Virulence* **12**, 312-328 (2021).
652 40. J. De Leon *et al.*, Mycobacterium tuberculosis ESAT-6 exhibits a unique
653 membrane-interacting activity that is not found in its ortholog from non-
654 pathogenic Mycobacterium smegmatis. *J Biol Chem* **287**, 44184-44191 (2012).

655 41. J. Jia *et al.*, Galectins Control mTOR in Response to Endomembrane Damage.
656 *Mol Cell* **70**, 120-135 e128 (2018).
657 42. K. B. Boyle, F. Randow, The role of 'eat-me' signals and autophagy cargo
658 receptors in innate immunity. *Curr Opin Microbiol* **16**, 339-348 (2013).
659 43. M. M. Osman *et al.*, Ebselen attenuates mycobacterial virulence through
660 inhibition of ESX-1 secretion. *bioRxiv* (2021).
661 44. C. Poulsen, S. Panjikar, S. J. Holton, M. Wilmanns, Y. H. Song, WXG100 protein
662 superfamily consists of three subfamilies and exhibits an alpha-helical C-terminal
663 conserved residue pattern. *PLoS One* **9**, e89313 (2014).
664 45. P. Brodin *et al.*, Functional analysis of early secreted antigenic target-6, the
665 dominant T-cell antigen of Mycobacterium tuberculosis, reveals key residues
666 involved in secretion, complex formation, virulence, and immunogenicity. *J Biol*
667 *Chem* **280**, 33953-33959 (2005).
668 46. Y. Ma, V. Keil, J. Sun, Characterization of Mycobacterium tuberculosis EsxA
669 membrane insertion: roles of N- and C-terminal flexible arms and central helix-
670 turn-helix motif. *J Biol Chem* **290**, 7314-7322 (2015).
671 47. R. Simeone *et al.*, Cytosolic access of Mycobacterium tuberculosis: critical
672 impact of phagosomal acidification control and demonstration of occurrence in
673 vivo. *PLoS Pathog* **11**, e1004650 (2015).
674 48. S. van der Niet *et al.*, IL-1R1-Dependent Signals Improve Control of Cytosolic
675 Virulent Mycobacteria In Vivo. *mSphere* **6** (2021).
676 49. J. F. Dermine *et al.*, Flotillin-1-enriched lipid raft domains accumulate on
677 maturing phagosomes. *J Biol Chem* **276**, 18507-18512 (2001).

678 50. S. Levitte *et al.*, Mycobacterial Acid Tolerance Enables Phagolysosomal Survival
679 and Establishment of Tuberculous Infection In Vivo. *Cell Host Microbe* **20**, 250-
680 258 (2016).
681 51. C. Vilcheze *et al.*, Rational Design of Biosafety Level 2-Approved, Multidrug-
682 Resistant Strains of Mycobacterium tuberculosis through Nutrient Auxotrophy.
683 *mBio* **9** (2018).
684 52. K. S. Beckwith *et al.*, Plasma membrane damage causes NLRP3 activation and
685 pyroptosis during Mycobacterium tuberculosis infection. *Nat Commun* **11**, 2270
686 (2020).
687 53. X. Peng, J. Sun, Mechanism of ESAT-6 membrane interaction and its roles in
688 pathogenesis of Mycobacterium tuberculosis. *Toxicon* **116**, 29-34 (2016).
689 54. J. Rengarajan, B. R. Bloom, E. J. Rubin, Genome-wide requirements for
690 Mycobacterium tuberculosis adaptation and survival in macrophages. *Proc Natl*
691 *Acad Sci U S A* **102**, 8327-8332 (2005).
692 55. C. M. Sassetti, E. J. Rubin, Genetic requirements for mycobacterial survival
693 during infection. *Proc Natl Acad Sci U S A* **100**, 12989-12994 (2003).
694 56. Y. J. Zhang *et al.*, Tryptophan biosynthesis protects mycobacteria from CD4 T-
695 cell-mediated killing. *Cell* **155**, 1296-1308 (2013).
696 57. P. A. Champion, Disconnecting in vitro ESX-1 secretion from mycobacterial
697 virulence. *J Bacteriol* **195**, 5418-5420 (2013).
698 58. P. S. Renshaw *et al.*, Structure and function of the complex formed by the
699 tuberculosis virulence factors CFP-10 and ESAT-6. *EMBO J* **24**, 2491-2498
700 (2005).

701 59. D. Houben *et al.*, ESX-1-mediated translocation to the cytosol controls virulence
702 of mycobacteria. *Cell Microbiol* **14**, 1287-1298 (2012).
703 60. O. S. Rosenberg *et al.*, Substrates Control Multimerization and Activation of the
704 Multi-Domain ATPase Motor of Type VII Secretion. *Cell* **161**, 501-512 (2015).
705 61. P. A. Champion, S. A. Stanley, M. M. Champion, E. J. Brown, J. S. Cox, C-
706 terminal signal sequence promotes virulence factor secretion in Mycobacterium
707 tuberculosis. *Science* **313**, 1632-1636 (2006).
708 62. E. N. Chernyaeva *et al.*, Genome-wide Mycobacterium tuberculosis variation
709 (GMTV) database: a new tool for integrating sequence variations and
710 epidemiology. *BMC Genomics* **15**, 308 (2014).
711 63. J. Jumper *et al.*, Highly accurate protein structure prediction with AlphaFold.
712 *Nature* **596**, 583-589 (2021).
713 64. D. Bottai *et al.*, ESAT-6 secretion-independent impact of ESX-1 genes espF and
714 espG1 on virulence of Mycobacterium tuberculosis. *J Infect Dis* **203**, 1155-1164
715 (2011).
716 65. Y. Lou, J. Rybniker, C. Sala, S. T. Cole, EspC forms a filamentous structure in
717 the cell envelope of Mycobacterium tuberculosis and impacts ESX-1 secretion.
718 *Mol Microbiol* **103**, 26-38 (2017).
719 66. A. Gijsbers *et al.*, Priming mycobacterial ESX-secreted protein B to form a
720 channel-like structure. *Curr Res Struct Biol* **3**, 153-164 (2021).
721 67. K. Takaki, J. M. Davis, K. Winglee, L. Ramakrishnan, Evaluation of the
722 pathogenesis and treatment of Mycobacterium marinum infection in zebrafish.
723 *Nat Protoc* **8**, 1114-1124 (2013).

724 68. S. Bardarov *et al.*, Specialized transduction: an efficient method for generating
725 marked and unmarked targeted gene disruptions in Mycobacterium tuberculosis,
726 M. bovis BCG and M. smegmatis. *Microbiology (Reading)* **148**, 3007-3017
727 (2002).
728 69. K. M. Guinn *et al.*, Individual RD1-region genes are required for export of ESAT-
729 6/CFP-10 and for virulence of Mycobacterium tuberculosis. *Mol Microbiol* **51**,
730 359-370 (2004).

731

Figure Legends

Figure 1. Minimal ESX-1 secretion is required for intramacrophage survival and virulence.

(**A**) Immunoblot of 48-hour Mm cell lysates and culture filtrates. Data representative of three independent experiments. GroEL2 is shown as a lysis control. (**B**) Contact-dependent hemolysis of red blood cells by Mm. Data combined from four experimental replicates. (**C**) Representative image of THP-1 cells infected with Mm, stained for galectin-8. Scale bar, 100 µm. (**D**) Percent of infected THP-1 macrophages with galectin-8 puncta. Each data point represents an individual imaging field. Horizontal lines, means. Statistics, one-way ANOVA with Šidák's multiple comparisons test. (**E**) Intramacrophage growth of Mm within J774A.1 cells as measured by bacterial fluorescence. Data representative of three independent experiments. (**F**, **G**, **H**) Zebrafish larvae at 5 dpi. Data representative of four independent experiments. (**F**) Representative images. Scale bar, 250 µm. Arrowheads, granulomas. (**G**) Bacterial burdens as assessed by bacterial fluorescence. (**H**) Average infection foci size per larva. Statistics, one-way ANOVA with Dunnett's test. (**I**) Contact-dependent hemolysis of red blood cells by Mm treated with vehicle or 16 µM Ebselen. Data combined from four experimental replicates. (**J**) Percent of infected THP-1 macrophages with galectin-8 puncta. Each data point represents an individual imaging field. Horizontal lines, means. Statistics, one-way ANOVA with Šidák's multiple comparisons test. (**K**) Intramacrophage growth of J774A.1 cells infected with Mm. Data representative of three independent experiments. (**E**, **K**) One-way ANOVA with Bonferroni's multiple comparisons test. Statistics, **** = $p<0.0001$, *** = $p\leq0.001$, ** = $p<0.01$, * = $p<0.05$, ns = $p>0.05$.

756 **Figure 2. ESAT-6 structures with C-terminal point mutations.**

757 (**A**) NMR structure of the heterodimer formed by ESAT-6 (blue) and CFP-10 (green)
758 (PDB 1WA8). N and C termini of ESAT-6 and CFP-10 are as labelled, as well as
759 methionine 83 and 93 of ESAT-6 (yellow). (**B**, **C**) Structure of ESAT-6 alone with
760 methionine residues 83 and 93 highlighted, as determined experimentally by NMR (**B**),
761 or the predicted model using AlphaFold2 (**C**).

762

763 **Figure 3. C-terminal point mutations in ESAT-6 support substantial levels of ESAT-**
764 **6 and CFP-10 secretion.**

765 (**A**, **B**) Immunoblots of 48-hour Mm cell lysates and culture filtrates. Representative of
766 three independent experiments. (**B**) Reprinted with permission from (8).

767

768 **Figure 4. ESAT-6 mediates phagosomal damage and virulence.**

769 (**A**) Contact-dependent hemolysis of RBC by Mm. Data combined from four
770 experimental replicates. (**B**) Percent of infected THP-1 macrophages with galectin-8
771 puncta. Each data point represents individual imaging fields. Horizontal lines, means.
772 Statistics, one-way ANOVA with Šidák correction for multiple comparisons. (**C**)
773 Intramacrophage growth of Mm within J774A.1 macrophages as measured by bacterial
774 fluorescence. Data representative of four independent experiments. (**D**,**E**,**F**) Zebrafish
775 larvae at 5 dpi. (**D**) Representative images. Scale bar, 500 μm. (**E**) Bacterial burdens as
776 assessed by bacterial fluorescence. Statistics, one-way ANOVA with Dunnett's test. (**F**)
777 Average infection foci size per larva. Statistics, one-way ANOVA with Dunnett's test.
778 Data representative of three independent experiments. Statistics, **** = $p<0.0001$, *** =
779 $p\leq0.001$, ns = $p>0.05$.

780

781 **Figure 5. Mm- and Mtb-mediated phagosomal membrane damage is enhanced in**

782 **acidified phagosomes.**

783 (**A**,**B**) Galectin-8 labeled, LysoTracker Red-stained THP-1 cells at 24 hours post-

784 infection with EBFP2-expressing Mm (top) or Mtb (bottom). (**A**) Representative images

785 of mycobacteria, Galectin-8, or Lysotracker, shown individually or as a merge of all three

786 channels. Scale bar, 10 μm. Magenta arrowhead, bacteria proximal to galectin-8 puncta.

787 Yellow arrowhead, acidified bacteria proximal to galectin-8 puncta. White arrowhead,

788 bacteria that did not induce galectin-8 puncta. (**B**) Percent of bacteria located proximal to

789 galectin-8 puncta, sorted by colocalization with LysoTracker-positive compartments.

790 Statistics, Fisher's exact test.

791

792 **Figure 6. Recombinant ESAT-6-M93T has wild-type levels of acidified liposome**

793 **lysis activity.**

794 Quantification of pH-dependent liposome lysis by 3 μM recombinant ESAT-6 as

795 measured by fluorescent ANTS release from DOPC liposomes. Statistics, one-way

796 ANOVA with Šidák's multiple comparisons test; **** = $p<0.0001$, ns = $p>0.05$. Data

797 combined from four experimental replicates.

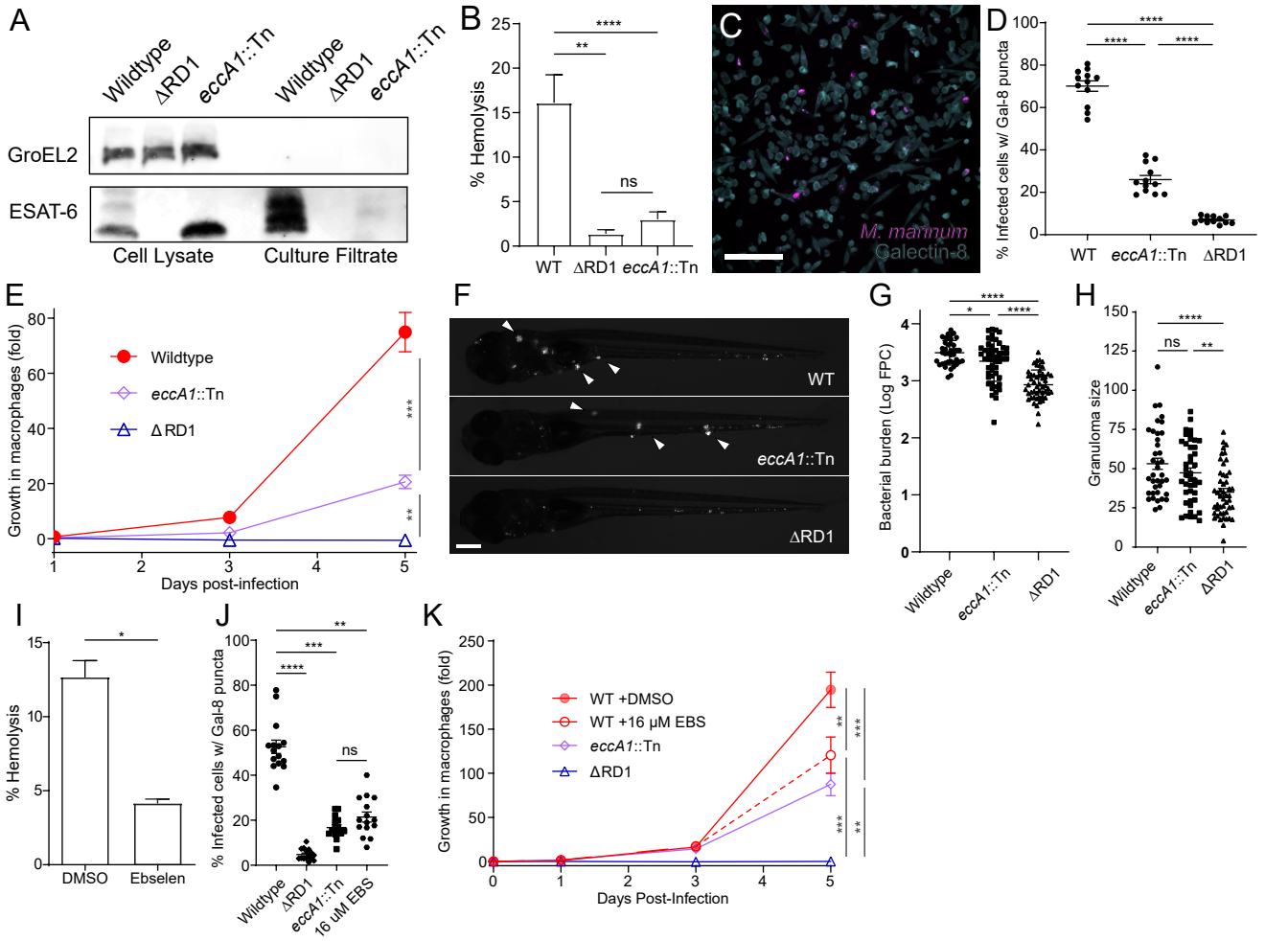
A
Wildtype
ΔRD1
eccA1::Tn
Wildtype
ΔRD1
eccA1::Tn
GroEL2
ESAT-6
Cell Lysate
Culture Filtrate
B
% Hemolysis
****
**
ns
WT
ΔRD1
eccA1::Tn
C
M. marinum
Galectin-8
D
% Infected cells w/ Gal-8 puncta
****
****
****
WT
eccA1::Tn
ΔRD1
E
Growth in macrophages (fold)
Wildtype
eccA1::Tn
ΔRD1
***
**
Days post-infection
F
WT
eccA1::Tn
ΔRD1
G
Bacterial burden (Log FPC)
****
*
****
Wildtype
eccA1::Tn
ΔRD1
H
Granuloma size
****
ns
**
Wildtype
eccA1::Tn
ΔRD1
I
% Hemolysis
*
DMSO
Ebselen
J
% Infected cells w/ Gal-8 puncta
**
***
****
ns
Wildtype
ΔRD1
eccA1::Tn
16 uM EBS
K
Growth in macrophages (fold)
WT +DMSO
WT +16 μM EBS
eccA1::Tn
ΔRD1
**
***
***
**
Days Post-Infection

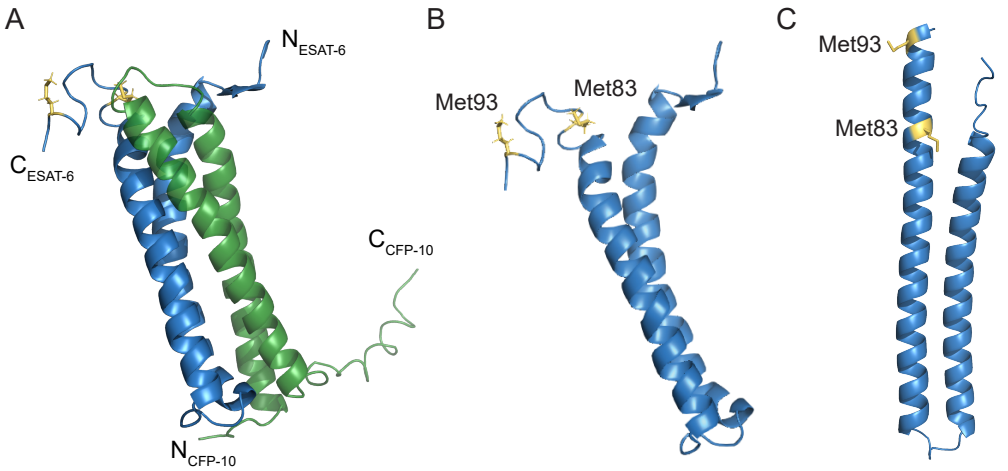
A
N ESAT-6
C ESAT-6
C CFP-10
N CFP-10
B
Met93
Met83
C
Met93
Met83

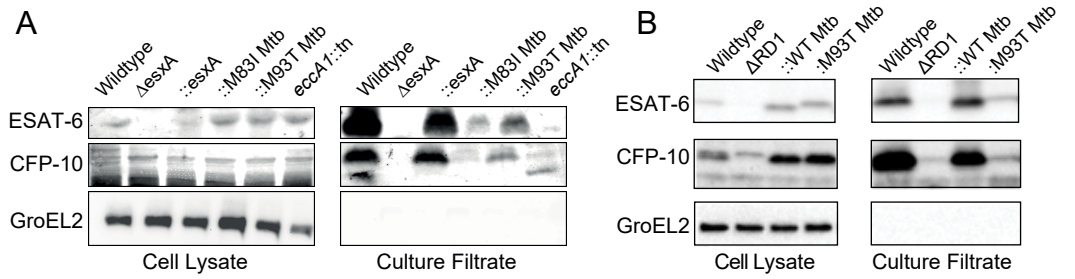
A
Wildtype
ΔesxA
::esxA
::M83I Mtb
::M93T Mtb
eccA1::tn
ESAT-6
CFP-10
GroEL2
Cell Lysate
Culture Filtrate
B
Wildtype
ΔRD1
::WT Mtb
::M93T Mtb
ESAT-6
CFP-10
GroEL2
Cell Lysate
Culture Filtrate

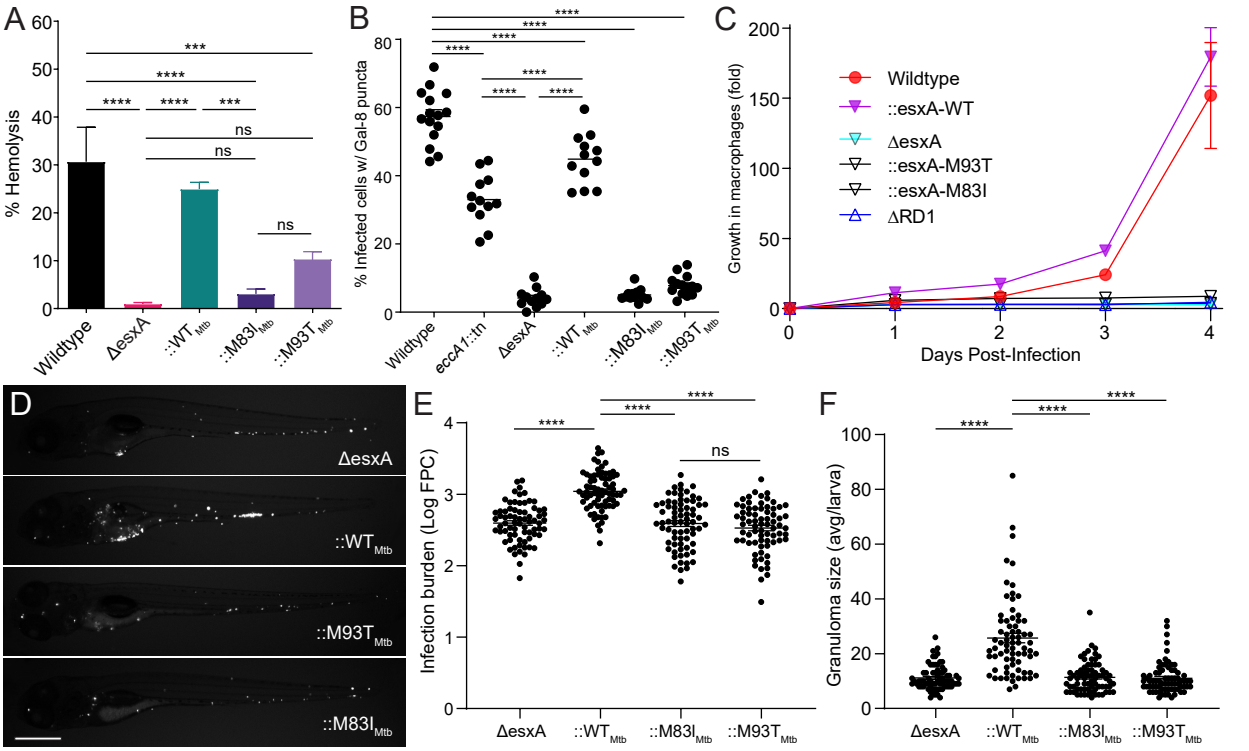
A
% Hemolysis
Wildtype
ΔesxA
::WTMtb
::M83IMtb
::M93TMtb
B
% Infected cells w/ Gal-8 puncta
eccA1::tn
C
Growth in macrophages (fold)
Days Post-Infection
Wildtype
::esxA-WT
ΔesxA
::esxA-M93T
::esxA-M83I
ΔRD1
D
ΔesxA
::WTMtb
::M93TMtb
::M83IMtb
E
Infection burden (Log FPC)
F
Granuloma size (avg/larva)

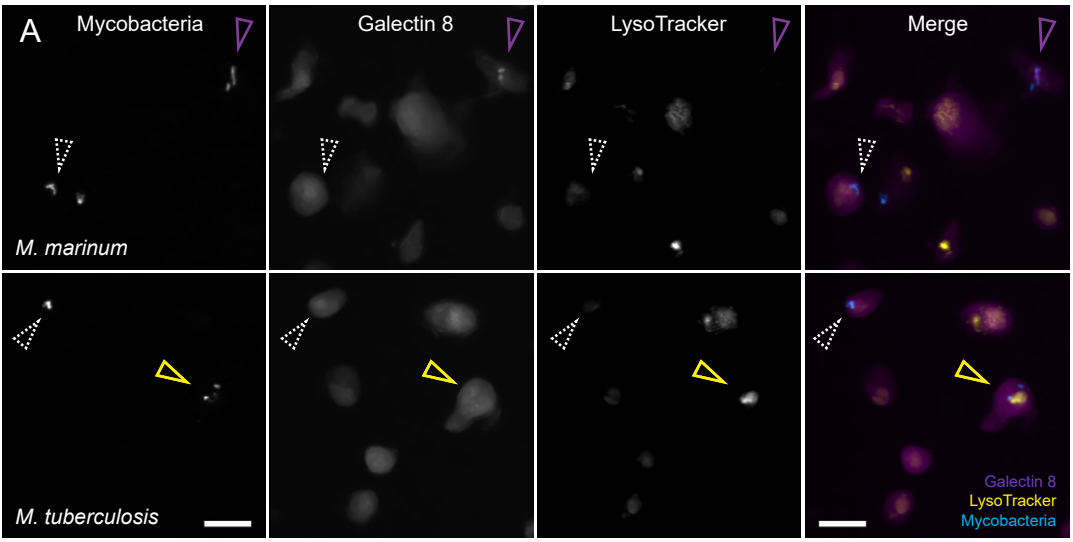
A
Mycobacteria
Galectin 8
LysoTracker
Merge
M. marinum
M. tuberculosis
Galectin 8
LysoTracker
Mycobacteria

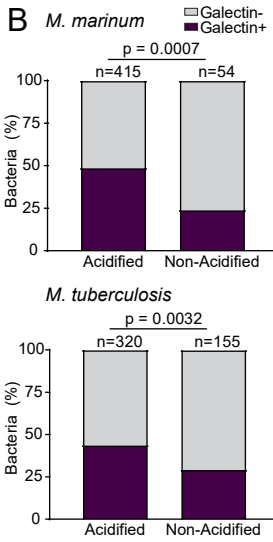
B
M. marinum
Galectin-
Galectin+
p = 0.0007
n=415
n=54
Bacteria (%)
100
75
50
25
0
Acidified
Non-Acidified
M. tuberculosis
p = 0.0032
n=320
n=155
Bacteria (%)
100
75
50
25
0
Acidified
Non-Acidified

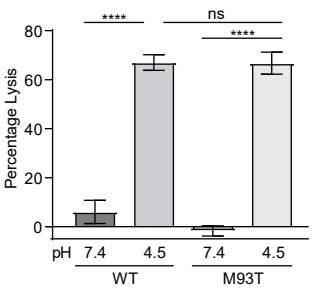
****
ns
****
80
60
40
20
0
Percentage Lysis
pH
7.4
4.5
7.4
4.5
WT
M93T

Supplementary Information for:

The C terminus of the mycobacterium ESX-1 secretion system substrate ESAT-6 is required for phagosomal membrane damage and virulence

Morwan M. Osman, Jonathan K. Shanahan, Frances Chu, Kevin Takaki, Malte L. Pinckert, Antonio Pagán, Roland Brosch, William H. Conrad, Lalita Ramakrishnan

This PDF file includes:

Supplementary Figures 1 to 3
Supplementary Tables 1 to 3
Supplementary References

Supplementary Figures

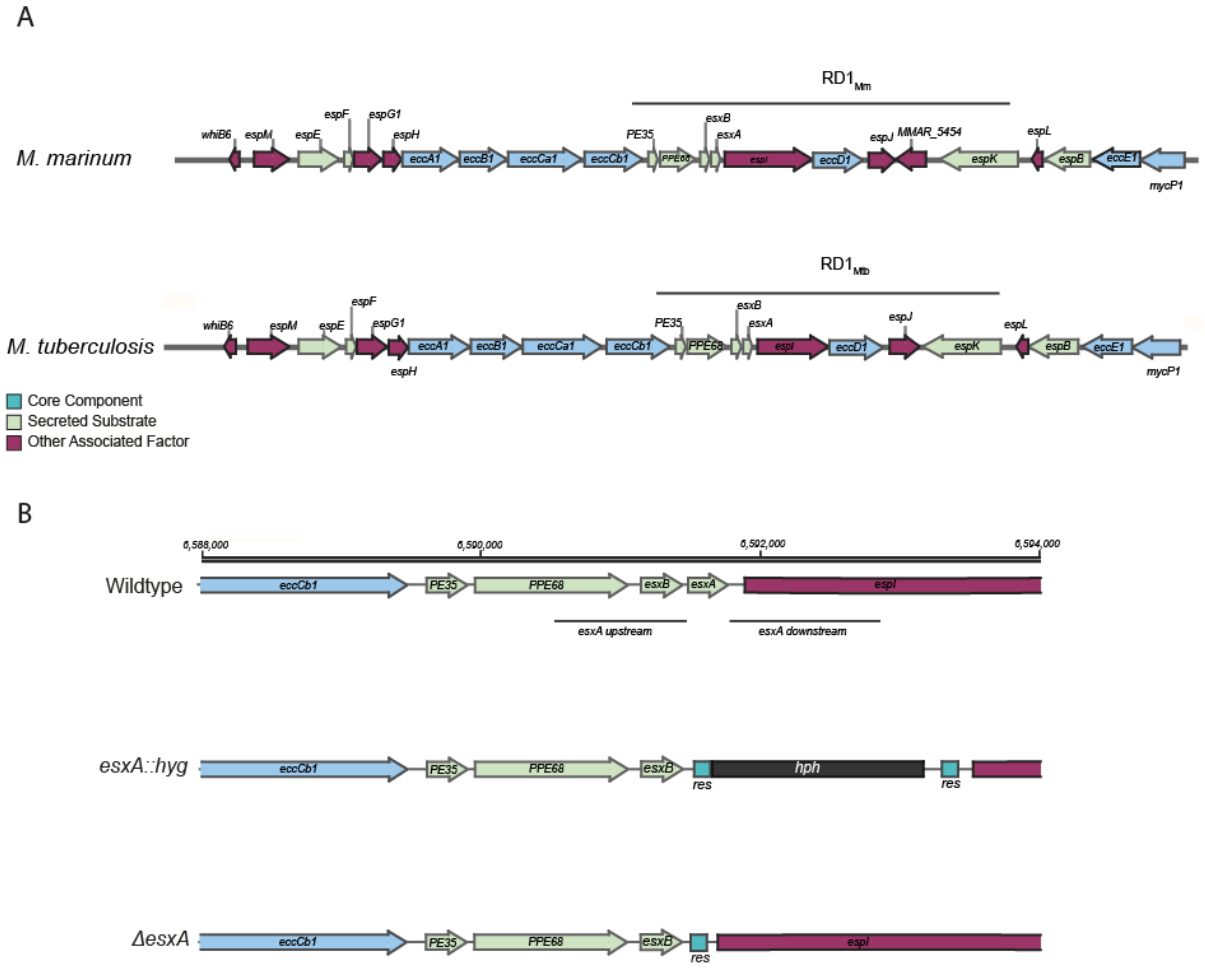

Figure S1. ESX-1 loci and scheme for Δ*esxA* mutant generation.
(**A**) Alignment of Mm and Mtb ESX-1 loci, with regions corresponding to RD1 deletions. (**B**) Schematic showing the initial, intermediate, and final alleles in the generation of the *esxA* mutant in Mm. (Top) Wildtype *esxA* loci with flanking region upstream and downstream *esxA* as targeted by the deletion construct. (Middle) Phage transduction was used to generate the *esxA::hyg* mutant with *esxA* replaced by the *res*-flanked *hph* gene encoding the hygromycin-B-phosphotransferase selectable marker. (Bottom) The *hph* gene was then excised by a gamma-delta resolvase, generating the unmarked Mm-*ΔesxA* mutant. Full details of the primers, plasmids and phasmids can be found in the Materials & Methods.

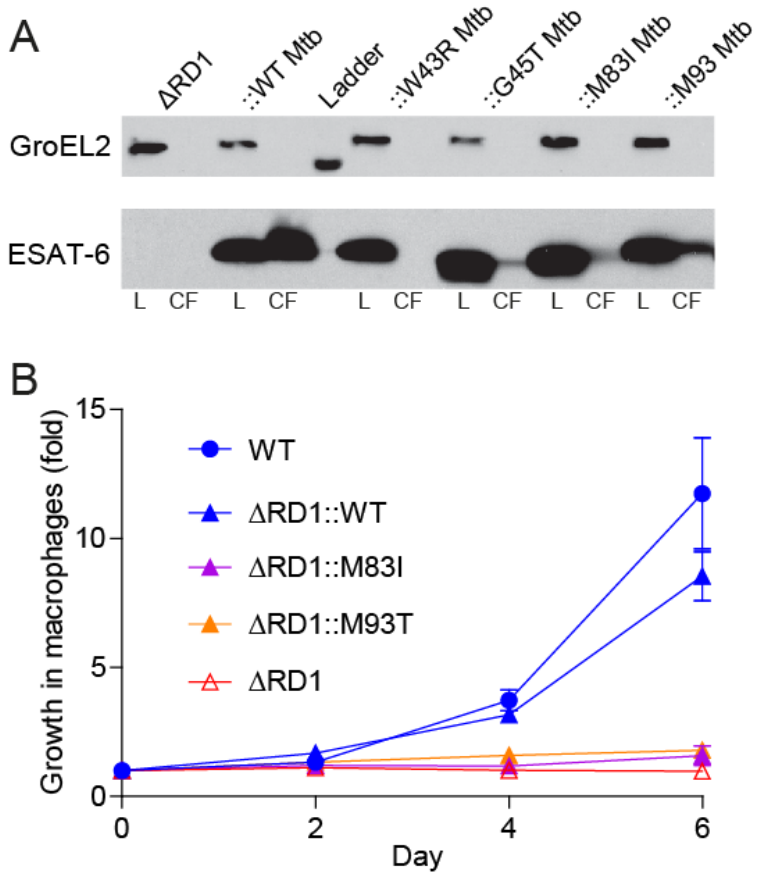

Figure S2. Mm ΔRD1::M83I$_{Mt}$ and ::M93T$_{Mt}$ mutants have reduced ESAT-6 secretion and fail to grow in macrophages.
(**A**) Immunoblot of Mm lysates (L) and culture filtrates (CF) at 48 hours. Data representative of three independent experiments. (**B**) Intramacrophage growth of Mm within J774A.1 cells as measured by bacterial fluorescence. Data representative of three independent experiments.

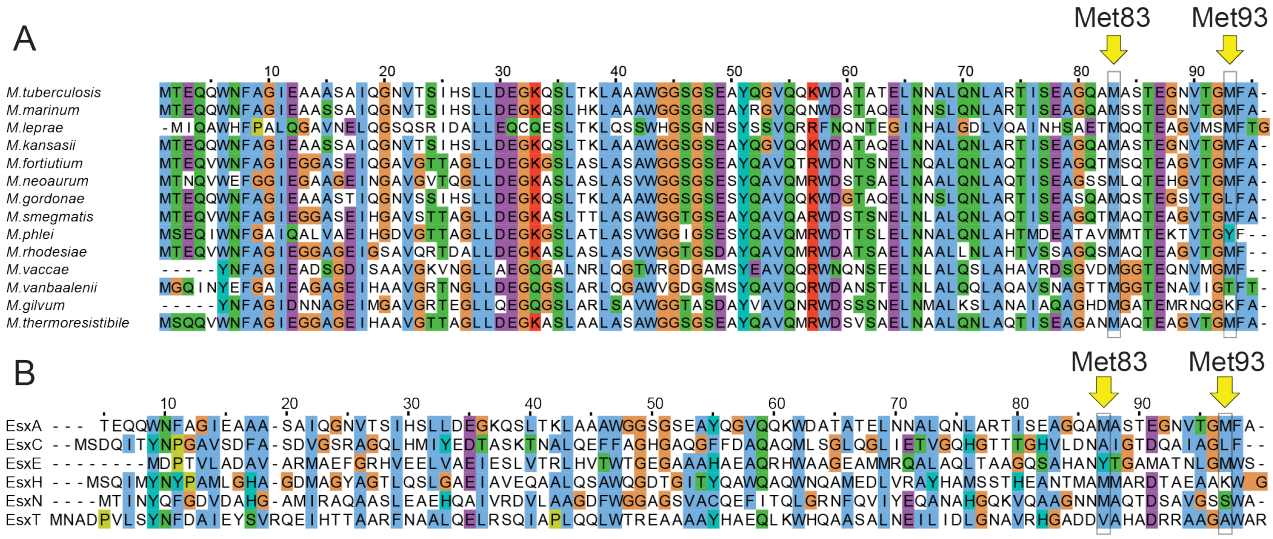

Figure S3. The C-terminal Met83 and Met93 residues of ESAT-6 are highly conserved. (**A**, **B**) Sequence alignment of Mtb ESAT-6 homologs (**A**) and paralogs (**B**). Yellow arrows denote residues aligned with Mtb ESAT-6 methionine 83 and 93.

55 # Supplementary Tables

56 **Table S1. Plasmids used in this study.**

57

Number	Plasmid	Use	Resistance	Source
1	pTEC27	Mycobacterial plasmid containing the gene for the fluorescent protein tdTomato under the constitutive mycobacterial promoter msp12.	Hygromycin	Addgene #30182
2	pTEC31	pTEC27 with the hygromycin resistance marker replaced with kanamycin.	Kanamycin	(1)
3	pTEC35	Mycobacterial plasmid expressing the fluorescence protein EBFP2 under the msp12 promoter.	Kanamycin	(1)
4	pMH406	Complementation construct containing *M. tuberculosis esxBA* operon under control of the mycobacterial optimal promoter	Kanamycin	(2)
5	pMH406-M83I	pMH406 with a point mutation resulting in the expression of ESAT-6 M83I	Kanamycin	This study
6	pMH406-M93T	pMH406 with a point mutation resulting in the expression of ESAT-6 M93T	Kanamycin	This study
7	ESAT-6-BEI	Purification of his-tagged EsxA	Ampicillin	BEI
8	CFP10-BEI	Purification of his-tagged EsxB	Ampicillin	BEI
9	pFC52	Expression of his-tagged EsxA mutant M93T.	Kanamycin	This study
10	phAE159	Shuttle phasmid for phage production.	Ampicillin	(3)
11	pYUB854	Contains a hygromycin cassette flanked by the γδ-resolvase sites.	Hygromycin	(3)
12	pYUB854-*esxA*	Plasmid 11 containing sequences upstream and downstream sequences flanking esxA.	Hygromycin	This study
13	phSP105	Plasmid 10 with PacI fragments from plasmid 12 subcloned in.	Hygromycin	This study
14	pYUB870	Plasmid containing the γδ-resolvase gene (*tnpR*) from transposon Tn1000 under the control of the mycobacterial *hsp60* promoter.	Kanamycin	(3)
15	2F9-*esxA*-WT	2F9 integrating cosmid containing the Mtb ESX-1 locus (bp 4,336,809-4,368,613).		(4)
16	2F9-*esxA*-W43R	Plasmid 15 with a mutation in *esxA* resulting in the production of ESAT-6-W43R.		(4)
17	2F9-*esxA*-G45T	Plasmid 15 with a mutation in *esxA* resulting in the production of ESAT-6-G45T		(4)
18	2F9-*esxA*-M83I	Plasmid 15 with a mutation in *esxA* resulting in the production of ESAT-6-M83I		(4)
19	2F9-*esxA*-M93T	Plasmid 15 with a mutation in *esxA* resulting in the production of ESAT-6-M93T		(4)

58

59 **Table S2. Primers used in this study.**
60

Primer Name	Sequence	Purpose
-955esxA_LF_SpeI_F	GCCACTAGTGTCACAGGTCACCGGCATAC	Cloning of upstream sequence of esxA for phage transduction.
-23esxA_LF_XhoI_R	GTTCCTCGAGCGTTTTAGGGGAATCAGAAGC	Cloning of upstream sequence of esxA for phage transduction.
+301esxA_RF_AgeI_F	AGGCACCGGTTTCGCGTAGAATACCGAAGC	Cloning of downstream sequence of esxA for phage transduction.
+1191esxA_RF_XbaI_R	GCCTCTAGAGGAGCCGGTGGCAGTT	Cloning of downstream sequence of esxA for phage transduction
esxA_SBprobe_F	GCATACCGAGCAGTGAGCTT	Southern blot probe for confirming insertion of hyg cassette into esxA
esxA_SBprobe_R	GCCAAATTGTTGGCAAGTCT	Southern blot probe for confirming insertion of hyg cassette into esxA
esxBA_Mm_Junct_F	gaggcaggtaatttcgagcg	PCR of Mm genomic region containing the junction between esxB and esxA
esxBA_Mm_Junct_R	ggtttgcccagtttcgtcat	PCR of Mm genomic region containing the junction between esxB and esxA
WC047	CTATGCGAACGTCCCAGTGAC	Site-directed mutagenesis of esxA to generate M93T
WC048	GTCACTGGGACGTTCGCATAG	Site-directed mutagenesis of esxA to generate M93T mutant
WC067	CTTCGGTCGAAGCTATTGCCTGACCG	Site-directed mutagenesis of esxA to generate M83I mutant
WC068	CGGTCAGGCAATAGCTTCGACCGAAG	Site-directed mutagenesis of esxA to generate M83I mutant
K2A	GGCCAGCGAGCTAACGAGACNNNNGTTGC	Arbitrary primer
K2B	GGCCAGCGAGCTAACGAGACNNNNGATAT	Arbitrary primer
K2C	GGCCAGCGAGCTAACGAGACNNNNAGTAC	Arbitrary primer
TnMarR3	ACAACAAAGCTCTCACCAACCGTG	Corresponds to one end of the TnMarMme transposon
K3	GGCCAGCGAGCTAACGAGAC	Fixed; corresponds to the set 5’ end of K2 primers
TnMarR2	CAGACACTGCTTGTCCGATATTTGATTTAGG	Corresponds to one end of the TnMarMme transposon (nested, internal to product produced by TnMarR3)

61
62

63

64 **Table S3. Mycobacterial strains used in this study.**

	Strain	Description	Resistance	Source
1	M strain	Wildtype M. marinum	None	ATCC
2	$mc^2$6206	*M. tuberculosis* H37Rv *ΔpanCD ΔleuCD,*	None	(5)
3	Δ*esxA*	M strain with a deletion of the *esxA* gene.	None	This study
4	*eccA1*::Tn	Transposon mutant 19729 containing transposon disrupting the *eccA1* gene	Hygromycin	This study
5	Δ*esxA::esxA*$_{Mtb}$	Strain 3 complemented with plasmid 4.	Kanamcyin	This study
6	Δ*esxA::esxA*-M83I$_{Mtb}$	Strain 3 complem::M93T$_{Mtb}$ ented with plasmid 5.	Kanamcyin	This study
7	Δ*esxA*::*esxA*-M93T$_{Mtb}$	Strain 3 complemented with plasmid 6. Also called ::M93T$_{Mtb}$	Kanamcyin	This study
8	Δ*esxA* + pTEC27	Strain 3 with plasmid 1.	Hygromycin	This study
9	Δ*esxA::esxA* + pTEC27	Strain 5 with plasmid 1	Hygromycin Kanamycin	This study
10	Δ*esxA::esxA*-M83I$_{Mtb}$ + pTEC27	Strain 6 with plasmid 1.	Hygromycin Kanamycin	This study
11	Δ*esxA*::*esxA*-M93T$_{Mtb}$ + pTEC27	Strain 7 with plasmid 1.	Hygromycin Kanamycin	This study
12	*eccA1*::Tn + pTEC31	Strain 4 with plasmid 2.	Hygromycin Kanamycin	This study
13	M strain + pTEC35	Wildtype M. marinum transformed with plasmid 3.	Kanamycin	This study
14	$mc^2$6206 + pTEC35	$mc^2$6206 transformed with plasmid 3.	Kanamycin	This study

65
66
67

68 **References:**

69 1. K. Takaki, J. M. Davis, K. Winglee, L. Ramakrishnan, Evaluation of the pathogenesis
70 and treatment of Mycobacterium marinum infection in zebrafish. *Nat Protoc* **8**, 1114-
71 1124 (2013).
72 2. K. M. Guinn *et al.*, Individual RD1-region genes are required for export of ESAT-
73 6/CFP-10 and for virulence of Mycobacterium tuberculosis. *Mol Microbiol* **51**, 359-
74 370 (2004).
75 3. S. Bardarov *et al.*, Specialized transduction: an efficient method for generating
76 marked and unmarked targeted gene disruptions in Mycobacterium tuberculosis, M.
77 bovis BCG and M. smegmatis. *Microbiology (Reading)* **148**, 3007-3017 (2002).
78 4. P. Brodin *et al.*, Functional analysis of early secreted antigenic target-6, the dominant
79 T-cell antigen of Mycobacterium tuberculosis, reveals key residues involved in
80 secretion, complex formation, virulence, and immunogenicity. *J Biol Chem* **280**,
81 33953-33959 (2005).
82 5. C. Vilcheze *et al.*, Rational Design of Biosafety Level 2-Approved, Multidrug-
83 Resistant Strains of Mycobacterium tuberculosis through Nutrient Auxotrophy. *mBio*
84 **9** (2018).

85